Chlorine Effects of Heterocyclic Ring-Based Donor Polymer for Low-Cost and High-Performance Nonfullerene Polymer Solar Cells

Sung Jae Jeon, Yong Woon Han, and Doo Kyung Moon*

The industrialization of polymer solar cells (PSCs) requires high-performance devices with high efficiencies and stabilities. Although high-performance PSCs are achieved via outstanding research into their component materials and device structures, several challenges still need to be overcome, including the synthetic complexity (SC) of producing the active material. In this study, donor polymers based on two heterocyclic rings and simple donor–acceptor structures are designed to obtain a low-cost material for PSCs. An inexpensive and high-performance donor polymer P(Cl) is realized by the introduction of a chlorine-atom substitution. P(Cl), which has lower SC than commercial donor polymers, has many advantages, such as high overall yield, low number of synthetic steps, and inexpensive raw materials. Moreover, fabricated P(Cl)-based PSCs exhibit a high power-conversion efficiency (PCE) of 12.14%. Through the shelf protocol of the international summit on organic photovoltaics stability in dark testing-1 (ISOS-D-1) measurements, superior long-term stability is demonstrated for P(Cl)-based devices both without and with encapsulation; their PCEs are maintained at 91% and 100% of the initial values for up to 2002 and 2858 h, respectively, under ambient conditions. Therefore, P(Cl) is a promising donor polymer for commercial PSC applications.

1. Introduction

Solution-processable polymer solar cells (PSCs) based on conjugated polymers have attracted much attention because of their advantages, such as low cost, flexibility, and lightweight; hence, they are regarded as potential renewable and sustainable energy sources for the near future.[1,2] The abundance of raw materials required for their fabrication and the ease of roll-to-roll processing make these conjugated polymers suitable for many applications, including packaging, clothing, semitransparent windows, and portable electronics.[3] The power-conversion efficiencies (PCEs) of bulk-heterojunction (BHJ) PSCs have steadily improved in the last two decades due to the development of new materials and device architectures and have recently reached over 15% for single solar cells, utilizing nonfullerene acceptors (NFAs) and over 17% for tandem solar cells.[4–9] Despite such impressive progress for PSCs, the high costs of raw materials and device fabrication remain to be solved.[10] In particular, the high cost of conjugated donor polymers is an important bottleneck issue for the development of PSCs; such costs mainly arise from the complexity of the synthetic steps, low overall yields, high raw materials costs, and the lack of scalability of the reaction for commercialization.[11,12] To address this issue, simplifying the molecular structure of the polymer to reduce the number of synthetic steps and improve the overall yield is considered to be a very effective strategy.

Recent studies on NFA-based PSCs make use of wide-bandgap conjugated donor polymer design strategies that contain 2D benzo[1,2-*b*:4,5-*b′*]dithiophene (2DBDT) derivatives and heterocyclic rings, due to the relative simplicity of their synthesis and refinement.[13–15] In 2017, Beaujuge and co-workers synthesized 2,5-dibromo-3,4-difluoro-thiophene from 2,5-dibromo thiophene using a three-step process. This was introduced to the design of a 2DBDT-based wide-bandgap polymer. The authors reported a maximum PCE of 9.8% by introducing fluorine, which generated a deep-lying highest occupied molecular orbital (HOMO) level, as well as improving charge generation and reducing geminate recombination.[14] In the same year, Choi and co-workers used thiophene-3-carboxylic acid as a raw material to synthesize methyl 2,5-dibromothiophene-3-carboxylate through two simple stepwise reactions. This was introduced to the design of a 2DBDT-based wide-bandgap polymer. They reported a maximum PCE of 9.73% for the polymer due to the increase in solubility for nonhalogenated solvents, caused by the conferring of regiorandom characteristics to the polymer through methyl carboxylate-substituted thiophene, which has an asymmetric structure.[13] These 2DBDT and heterocyclic ring-based polymer design strategies can dramatically reduce synthetic complexity (SC) through structural simplification; however, a trade-off between cost and efficiency is inevitable because only the limited number of functionalization and modification processes can be achieved at low cost.

S. J. Jeon, Y. W. Han, Prof. D. K. Moon
Nano and Information Materials (NIMs) Laboratory
Department of Chemical Engineering
Konkuk University
120, Neungdong-ro, Gwangjin-gu, Seoul 05029, Korea
E-mail: dkmoon@konkuk.ac.kr

The ORCID identification number(s) for the author(s) of this article can be found under https://doi.org/10.1002/solr.201900094.

Halogenation is one of the most efficient chemical modification strategies, and it has created many excellent donor and acceptor materials.[5,6,14–18] The electronegativity (EN) of halogen atoms follows the order of of F (4.0) > Cl (3.2) > Br (3.0) > I (2.7). Among these atoms, F is the most electronegative and has a very small size. Therefore, it can effectively control the properties of the π-electrons in the molecular structure and reduce the occurrence of steric hindrance during molecular packing.[19,20] Furthermore, in materials that contain F, noncovalent interactions in inter- and intramolecular structures occur; as a result, these materials may have better properties than those that do not contain F.[19] However, fluorination is often inappropriate for low-cost PSCs due to the need for relatively expensive reagents and complex synthesis and purification processes; moreover, it imparts a low yield.[14–16,21] Recent studies have demonstrated the excellent effects of halogen atoms other than F and their suitability for various molecular structure design goals, irrespective of the EN order.[18]

In this study, we introduce monohalogenated heterocyclic rings to 2DBDT to enable effective interchain π—π stacking and systematically design them to develop low-cost and high-performance wide-bandgap donor polymers. Before material synthesis, the B3LYP/3-21G$^{(*)}$ function of Gaussian 09 was used to calculate the HOMO, lowest unoccupied molecular orbital (LUMO), bandgap (E_g), and dipole moment (D) of 2DBDT, thiophene, and halogenated thiophene units (see Supporting Information, Chart S1).

The Gaussian calculation results show that 3-chlorothiophene (Th–Cl) has the best characteristics among the halogenated thiophene units (Th–F, Th–Cl, Th–Br, and Th–I) and the nonhalogenated thiophene unit (Th). In particular, the dipole moment becomes larger in the order of Th (H, 0.533) < Th–Br (1.031) < Th–I (1.041) < Th–F (1.161) < Th–Cl (1.454). The 2DBDT, which has a centrosymmetric structure, has a dipole moment of 0; therefore, the net dipole moment of designed polymers is determined by the dipole moment of the monohalogenated heterocyclic rings. Although Th–Cl has an EN that is approximately 0.8 less than that of Th–F, the selection of Th–Cl, which has great advantages in terms of the overall synthetic steps, operation units, yields, and so on, is inevitable if one takes finance into consideration (Scheme S1, Supporting Information).

To closely examine the effects of Cl on polymers designed based on 2DBDT-monohalogenated thiophene, two types of polymers, P(Th) and P(Cl) (i.e., without and with Cl, respectively), were synthesized, and various properties, including physical, optical, electrochemical, photovoltaic, and morphological properties, were investigated according to whether or not Cl was introduced. By optimizing both polymers with 3,9-bis(2-methylene-(3-(1,1-dicyanomethylene)-indanone))-5,5-11,11-tetrakis(4-hexylthienyl)-dithieno[2,3-*d*:2′,3′-*d*′]-s-indaceno[1,2-*b*:4,5-*b*′]dithiophene (ITIC-Th) in an inverted structure, P(Th) showed a maximum PCE of 2.6%, whereas P(Cl) showed a maximum PCE of 12.14%, as certified by the Nano Practical Application Center (NPAC) in Korea. Furthermore, PSC devices incorporating P(Cl), without and with encapsulation, showed no reduction in the initial parameters over a shelf lifetime of over 300 h; in addition, the devices exhibited excellent stability. Moreover, both devices show a trend of increasing efficiency with time, with maximum PCEs of 11.3% and 11.4% at 167 and 246 h after the devices were fabricated, respectively. Even after 2000 h, both devices, without and with encapsulation, show efficiency decreases of 9.3% and −1.0%, respectively, compared with the initial efficiency.

2. Results and Discussion

2.1. Design, Theoretical Calculations, and Physical Properties

We successfully synthesized two similar donor polymers for P(Th) and P(Cl) based on 2DBDT-heterocyclic rings (**Scheme 1**). 4,8-Bis[5-(2-ethylhexyl)thiophen-2-yl]-2,6-bis(trimethylstannyl)benzo-[1,2-*b*:4,5-*b*′]dithiophene (M1) and 2,5-dibromothiophene (M2) were purchased at low cost from commercial sources and used for the polymerization without refinement, and 2,5-dibromo-3-chlorothiophene (dibromo-Th–Cl) was easily synthesized in just one round of synthesis and refinement from an inexpensive raw material, 3-chlorothiophene, with a high yield of 95.2%, for use in the polymerization (Figure S1–S5, Supporting Information). The structures of the two polymers only differ in terms of whether or not there is chlorothiophene in the polymer backbone; this, however, causes a major difference in the number of possible conformations (Figure S6, Supporting Information). P(Th) has a regioregular structure due to alternating polymerization between centrosymmetric 2DBDT and axisymmetric thiophene units and prefers to adopt only one possible conformation even if the number of repeating units increases; in contrast, because of the introduction of asymmetric chlorothiophene, P(Cl) has the regiorandom segments, and more structural irregularities occur during polymerization. As the number of repeating units increases, the number of possible conformations increases correspondingly one by one.[22,23]

To examine these differences more closely, simulations were performed using Gaussian 09 software for P(Th) and P(Cl) with a repeating unit of $n = 1$. P(Cl) is distinguished by the orientation of the Cl direction with respect to the rest of the unit, which takes "in" (P(Cl)-in) or "out" (P(Cl)-out) conformations; both these possibilities were computed. First, to determine the optimized structure for the combined 2DBDT and thiophene/chlorothiophene unit, the total energy was computed while scanning the dihedral angle (Figure S7, Supporting Information). As a result, P(Th), P(Cl)-in, and P(Cl)-out showed two stabilized energy states, with minimized total energies at dihedral angles ($θ$) of 10°, 20°, and 30°, respectively, and different optimized geometries. The reason these differences occurred was the introduction of Cl, which is more bulky than H, causing a large amount of tilting within the molecular structure[5,6,16,17] (Figure S7a and b, Supporting Information). The electrostatic potential (ESP) and dipole moment of each optimized structure were calculated (Figure S7c, Supporting Information). As shown in the ESP results, there are dominant continuous positive charges along all the main conjugated backbones of the P(Th), P(Cl)-in, and P(Cl)-out structures, which means that charge-carrier transport occurs along the backbones.[24] The dipole moments of P(Cl)-in and P(Cl)-out were computed to be 1.240 D and 1.862 D, respectively, which are around twice that of P(Th) (0.740 D). Therefore, it is expected that the P(Cl)-in/out structure will provide improved charge separation and transport compared with P(Th).[25]
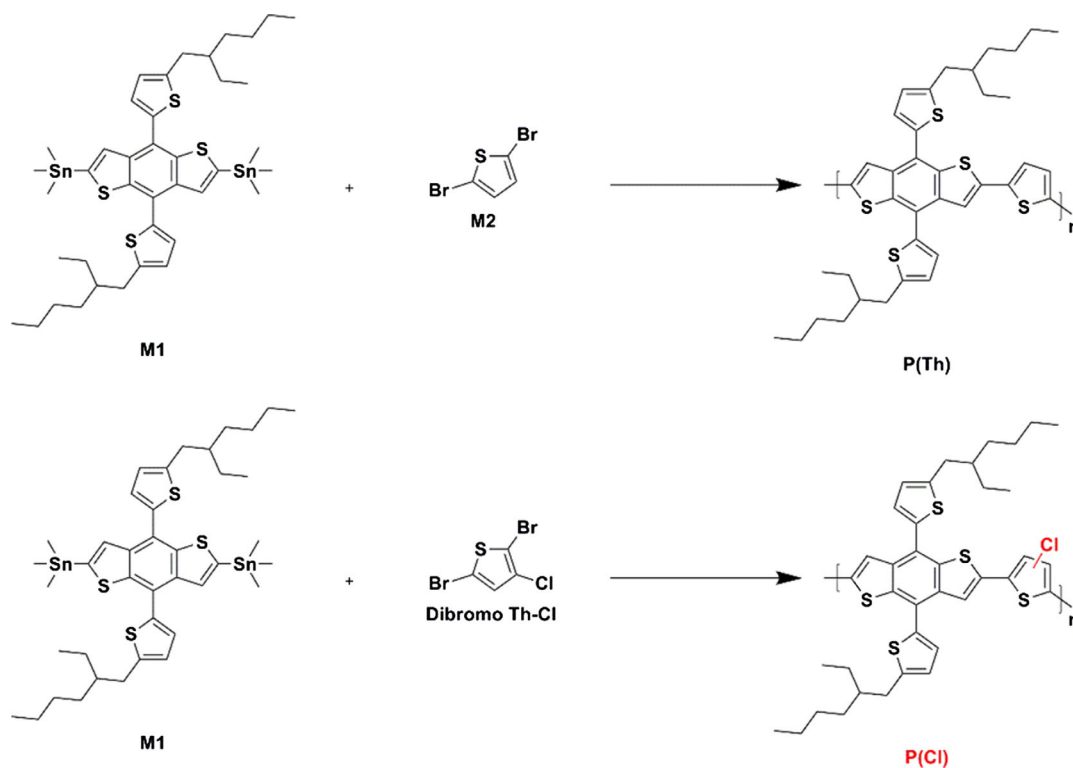
Scheme 1. Synthesis routes to the polymers P(Th) and P(Cl).

Next, to perform a more accurate comparison of the conformational differences between the polymers, density functional theory (DFT) calculations were performed in polymers with $n = 2$ (Figure S8 and Table S1, Supporting Information). Calculation of the dihedral angles (θ_1, θ_2, and θ_3) and LUMO and HOMO levels of the polymers showed that P(Th) has twisted and linear curvatures, with 14.4° for θ_1, 15.3° for θ_2, and 14.1° for θ_3. In contrast, the regiorandom (RA) structures 1 and 2 for P(Cl) (denoted as P(Cl)-RA1 and P(Cl)-RA2, respectively) and the regioregular structure for P(Cl) (denoted as P(Cl)-RR) both showed more twisted and zig-zagged curvatures because of the higher tilt angles in the range of 22.7–32.6° between chlorothiophene and the adjacent 2DBDT because of the large size of Cl. Furthermore, due to the effects of Cl, P(Cl) structures containing P(Cl)-RA1, P(Cl)-RA2, and P(Cl)-RR demonstrated HOMO levels of −5.018, −5.058, and −5.043 eV, respectively, which are downshifted by 0.13–0.17 eV compared with that of P(Th) (−4.890 eV). Therefore, the HOMO of the P(Cl) polymer is better aligned than that of P(Th) with the LUMO energy levels of ITIC derivatives, and a high open-circuit voltage (V_{oc}) can be expected when fabricating devices using P(Cl). The bandgaps of model compounds for P(Cl) structures show a tendency to increase slightly compared with those of P(Th) in the case of regiorandom structures and decrease slightly in the case of regioregular structures. An experimental polymer behavior showed that the bandgap of P(Cl) is reduced relative to that of P(Th). This means that in P(Cl), which was synthesized via a conventional one-pot polymerization reaction, more regioregular than regiorandom segments were formed in the polymer backbone. This is in agreement with the results of a study by Jen and

co-workers on the regio- and chemoselectivity of polymers composed of fluoro-substituted thienothiophene, which has an asymmetric structure, and 2DBDT, which is centrosymmetric. It has been reported that polymers obtained by conventional one-pot Stille C—C coupling of these structures have a 0.36/0.65 ratio of regiorandom to regioregular segments.[26] To understand the polymer behaviors of P(Th) and P(Cl), the ESP along the conjugated polymer backbones with $n = 4$ was calculated (**Figure 1**). Unlike the case of $n = 1$, clear changes in the positive and negative charges along the main conjugated backbones of P(Cl)-RA and P(Cl)-RR are revealed, and a higher push–pull-type charge potential compared with P(Th) is manifested for these structures.[27–29] In the case of P(Th), the H···S interaction between thiophene H and the adjacent S of 2DBDT is weaker than the Cl·S interactions of P(Cl)-RA or P(Cl)-RR. As the distances between the monomers increase from 2.96 Å (in P(Cl)) to 3.33 Å (in P(Th)), due to this difference in the interaction strength, strong localization occurs and a partial negative charge at Cl·S is seen.[29] The most negative ESPs on groups in the molecule can induce electrostatic interactions inside and outside it, or with the relative acceptor, and an improvement in charge transport due to charge dissociation can be expected.[28,29]

The molecular weights of the polymers were determined via gel-permeation chromatography (GPC) using chloroform (CF) as an eluent at room temperature; the results are shown in **Table 1** (Figure S9, Supporting Information). All the polymers have relatively high weight-average molecular weights ($M_w \geq 25$ kDa).[5,19–21] It has been reported that the weight-average molecular weight of a polymer could influence its photovoltaic properties, with larger values enhancing the aggregation behavior.[30] In this study, the
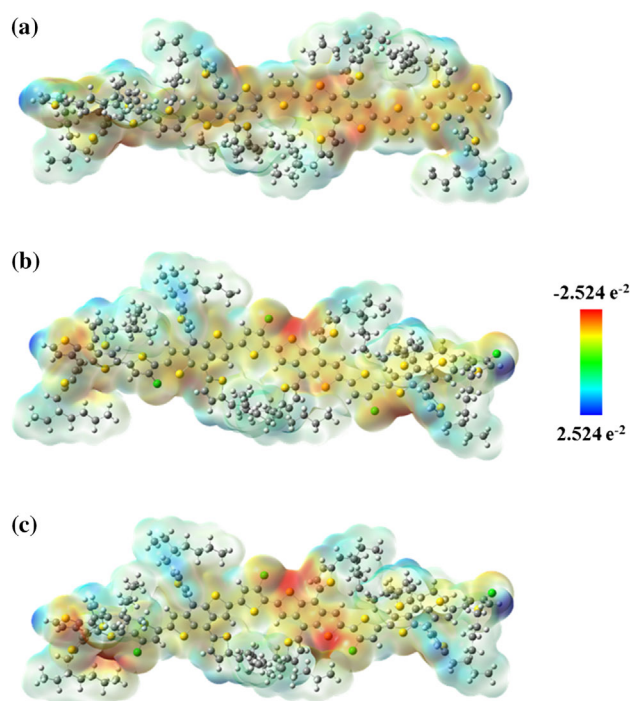
Figure 1. Calculated ESP surfaces of the polymers with $n = 4$: a) P(Th), b) P(Cl)-RA, and c) P(Cl)-RR.

Table 1. Physical and thermal properties of P(Cl) and P(Th) polymers.

Polymer	Yield [%]	M_n[a] [kDa]	M_w[a] [kDa]	PDI[a]	T_d[b] [°C]
P(Th)	67.0	17.3	25.4	1.47	330
P(Cl)	90.0	38.1	82.5	2.17	350

[a]The parameters (M_n: number-average molecular weight; PDI: polydispersity index) determined by GPC in CF using polystyrene standards; [b]Temperature resulting in 5% weight loss based on the initial weight.

obtained experimental weight-average molecular weights of P(Cl) are greater than those of P(Th) by a factor of more than two. This is due to the difference in structural irregularities caused by the selection of axisymmetric thiophene and asymmetric chlorothiophene, which are relative monomer units of the centrosymmetric 2DBDT unit that participates in the polymerization, as discussed previously. P(Cl), which has a relatively high structural irregularity, was able to form a polymer of a higher molecular weight than P(Th).[22,31] Both polymers dissolve well in common organic solvents, such as CF, chlorobenzene (CB), and dichlorobenzene (DCB).

The thermal properties of these polymers were analyzed by a thermogravimetric analysis (TGA) (Table 1). P(Th) is thermally stable up to 330 °C (5% weight-loss temperature), whereas P(Cl) shows thermal stability up to 350 °C, which is a 20 °C improvement (Figure S10, Supporting Information). These results indicate that the thermal stability of the polymers is sufficiently high for their application in PSCs.[13,20] In addition, the results of differential scanning calorimetry (DSC) on the polymers showed that neither polymer had discernible glass-transition

characteristics up to 270 °C, and it is known that they have an amorphous nature[32] (Figure S11, Supporting Information).

2.2. Optical and Electrochemical Properties

The optical and electrochemical properties of the polymers were investigated both in CF and in thin films (**Figure 2**). To help understand the optical and electrochemical interactions between the polymers and the NFAs, an NFA, ITIC-Th, was also analyzed in this study. Figure 2a shows the average molar absorption coefficients of the polymers and ITIC-Th, each measured in a 10^{-5} M CF solution. Figure 2b shows UV–visible absorption spectra of the polymers and ITIC-Th in CF thin films, and Figure 2c shows the cyclic voltammetry (CV) curves. Both polymers showed three principle features in their absorption spectra: the first band, located at 361–369 nm, is assigned to π—π* transitions; the second band, at 525–530 nm (in the long-wavelength region), corresponds to intramolecular charge transfer (ICT) between the 2DBDT and thiophene units of the polymers;[20] the third band is seen as a vibronic shoulder in the spectra of both polymers, but, it is clearer for the polymer to which chlorine was introduced.[5,16,17]

To closely examine the inherent absorption properties of the polymers and ITIC-Th, the Beer–Lambert equation ($A = \varepsilon bc$; A: absorbance; ε: molar absorption coefficient of the dye; b: length of the light path; and c: concentration of the dye in solution) was used to calculate the average value of ε from four different CF solutions, as shown in Figure 2a (Figure S12, Supporting Information). The results for P(Th) were 20 605, 42 680, and 36 454 $M^{-1}\,cm^{-1}$ at λ_{max} of 369, 525, and 559 nm, respectively. The results for P(Cl) were 27 837, 70 617, and 67 929 $M^{-1}\,cm^{-1}$ at λ_{max} of 361, 530, and 562 nm, respectively. In the long-wavelength region where ICT is manifested, the maximum wavelengths had reasonable molar absorption coefficients over 30 000 for both polymers, which means they have a good capacity for harvesting solar photons if blended with ITIC-Th because of its high ε of 111 959 $M^{-1}\,cm^{-1}$ at λ_{max} of 670 nm.[14,16,21,33] P(Cl) has a molar absorption coefficient that is more than 1.5 times higher than that of P(Th) in the long-wavelength region because P(Cl) has a relatively high molecular weight, EN, and dipole movement.[10,16,18]

Next, we consider the UV absorption of the polymers and ITIC-Th in the thin-film state (Figure 2b). In the solid state, P(Th) does not experience a red-shift, but P(Cl) shows clear red-shifts of 5–16 nm for all the peak values. These differences indicate that self-aggregates or ordered assemblies are formed in the solid state through intermolecular π—π stacking interactions.[5,6,13] In addition, the absorption spectra of P(Cl) display a stronger vibronic shoulder peak than those of P(Th) both in the solution and film states, which is probably due to the higher molecular weight and increased intermolecular interactions between the polymer backbones of P(Cl).[30,34] This pronounced shoulder suggests the existence of stronger π—π stacking effects for P(Cl), which may be beneficial for charge-carrier mobility in the resulting polymer films.[5] The optical bandgaps (E_g^{opt}), determined from the absorption onset of the polymer and ITIC-Th films, are 2.03, 1.97, and 1.60 eV, respectively, for P(Th), P(Cl), and ITIC-Th, respectively. Thus, P(Cl) was found to have more complementary absorption characteristics for those of ITIC-Th in the vis–near-IR (NIR) region than P(Th).
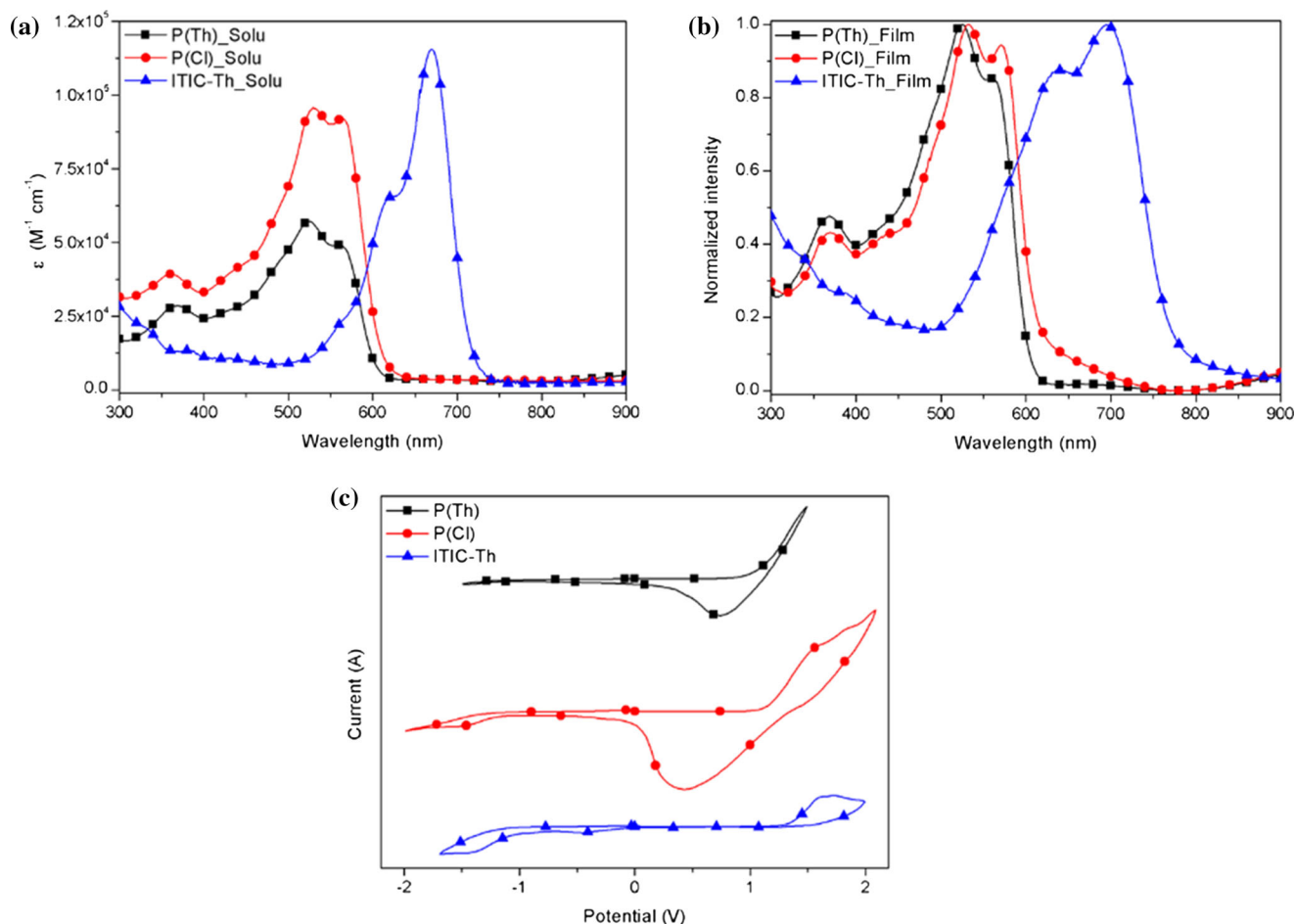
Figure 2. UV–visible absorption and CV spectra of P(Th) and (PCl) polymers and ITIC-Th: a) average molar absorption coefficients for dilute CF solutions, b) UV–visible absorption spectra of CF thin films, and c) CV curves for the CF thin films.

Finally, as shown in Figure 2c, the HOMO and LUMO energy levels of the polymers and ITIC-Th were determined from the onset oxidation potential (E_{ox}^{onset}) and E_g–E_{HOMO}, respectively, and by using the following electrochemical equation: $E_{HOMO} = -4.8 - (E_{ox}^{onset} - E_{1/2,ferrocene})$, where $E_{1/2,ferrocene} = 0.49$ eV (measured data). Our results revealed that the corresponding HOMO energy levels of P(Th) and P(Cl) were −5.32 and −5.47 eV, respectively, meaning that the HOMO of P(Cl) is around −0.15 eV lower than that of P(Th). Because of the substitution of the electron-deficient Cl atom, the HOMO of the P(Cl) polymer became less than that of P(Th).[5,6,16] These factors will definitely increase the V_{oc} value of the P(Cl) and ITIC-Th combination,[5] and these results correspond very well with the results of the DFT calculations described in Section 2.1. Therefore, P(Cl) is beneficial for chemical stability and for obtaining higher V_{oc} values in PSCs. **Table 2** lists the details of the optical and electrochemical properties of the materials.

2.3. Photovoltaic Performance

To investigate the photovoltaic properties of the polymers and ITIC-Th, inverted device configurations of ITO/ZnO/polymer:

ITIC-Th/MoO$_3$/Ag were fabricated. Detailed information on the devices is given in the Supporting Information; to aid understanding, the energy-level diagrams of the active layer are shown in the structure shown in the Supporting Information (Figure S13, Supporting Information). We chose an inverted device configuration because the high work function metal anode allows for improved device stability.[35] In the case of P(Cl), the performances of the devices were fully characterized and optimized according to the order: thermal annealing (TA), thickness, types of NFAs , donor and acceptor (D:A) ratios, solution concentrations, and volume of 1,8-diiodooctane additive (Figure S14–S18 and Table S2–S7, Supporting Information). The current density–voltage (J–V) and external quantum efficiency (EQE) curves of the optimized polymer blends are shown in **Figure 3**a,b, respectively, and the associated parameters are listed in **Table 3**. As shown in Figure 3a and Table 3, the P(Th):ITIC-Th-based optimized device shows a PCE of 2.6% with a V_{oc} value of 0.779 V, a short-circuit current density (J_{sc}) of 8.8 mA cm^{-2}, and a fill factor (FF) of 37.3% at an 85-nm thickness. In contrast, the optimized P(Cl):ITIC-Th device shows a PCE of 10.8% with a V_{oc} value of 0.859 V, a J_{sc} value of 18.2 mA cm^{-2}, and an FF of 68.9% at a thickness of 120 nm. This device was then encapsulated and aged in an air atmosphere for 246 h. As a result, it was

Table 2. Optical and electrochemical properties of polymers and ITIC-Th.

Polymer	UV–visible absorption			CV			
	CF solution, λ_{max} [nm]	Molar absorption coefficient, ε [M^{-1} cm^{-1}] at λ_{max} [nm]	Film, λ_{max} [nm]	$E_g^{opt\,a)}$ [eV]	E_{ox}^{onset} [V]	$E_{HOMO}^{b)}$ [eV]	$E_{LUMO}^{b)}$ [eV]
	369	20 605 (369)	369				
P(Th)	525	42 680 (525)	525	2.03	1.01	−5.32	−3.32
	559	36 454 (559)	559				
	361	27 837 (361)	376				
P(Cl)	530	70 617 (530)	535	1.97	1.16	−5.47	−3.50
	562	67 929 (562)	578				
ITIC-Th	670	111 959 (670)	695	1.60	1.34	−5.65	−4.05

[a)]Calculated from the intersection of the tangent on the low energetic edge of the absorption spectrum with the baseline; [b)]$E_{HOMO} = -[E_{ox}^{onset}$ (vs Ag/AgCl) $- E_{1/2}$(Fc/Fc$^+$ vs Ag/AgCl)[c)]] $- 4.8$ eV, $E_{LUMO} = E_g^{opt} - E_{HOMO}$; [c)]$E_{1/2}$(Fc/Fc$^+$ vs Ag/AgCl) $= 0.49$ eV (measured data).
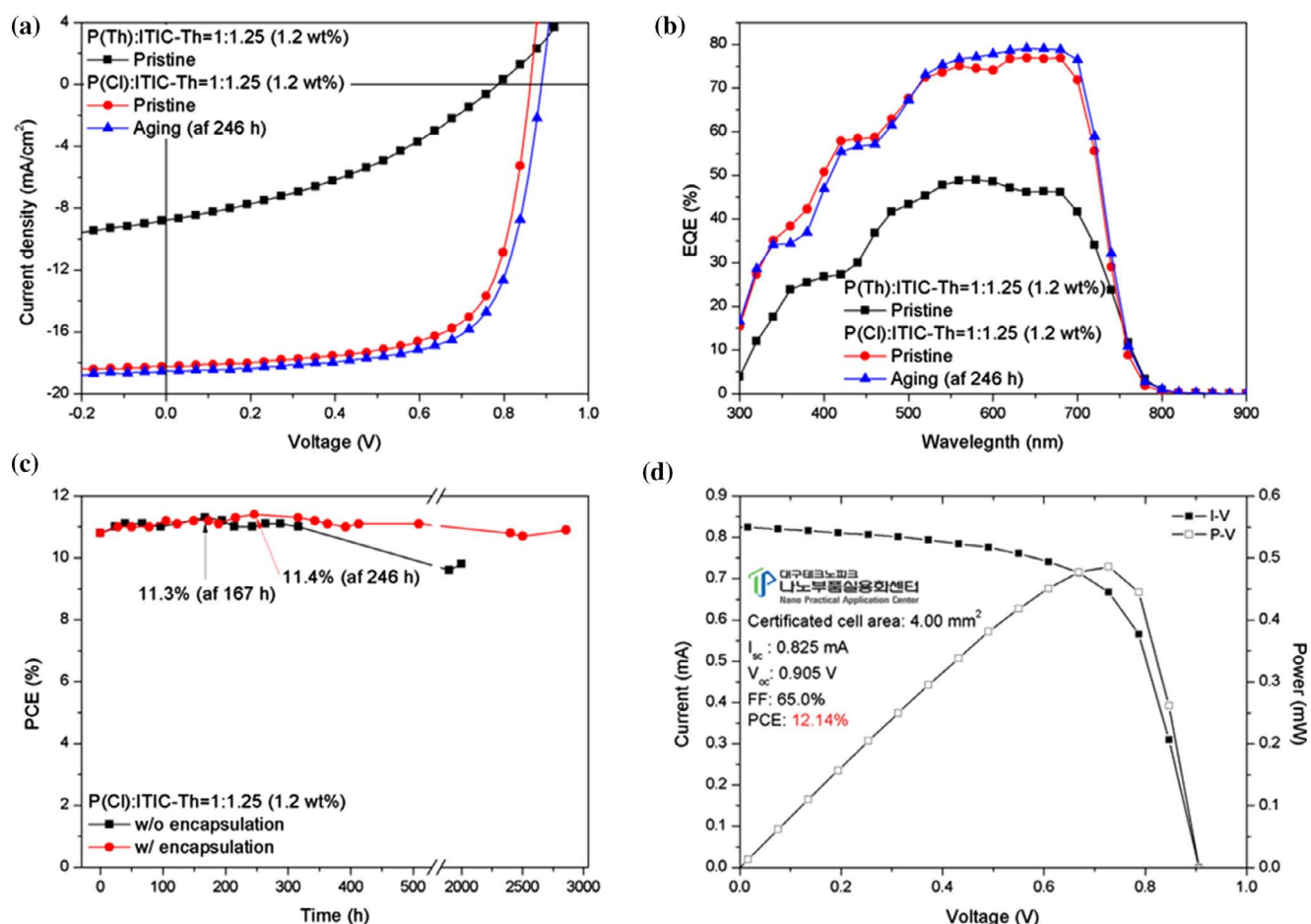

Figure 3. a) J–V curves, b) EQE curves, and c) long-lifetime stability results obtained using the ISOS-D-1 (shelf) protocol for the optimized polymer blends used in inverted PSCs. d) The photovoltaic results of the best-efficiency device as certified by the NCPAC in the Republic of Korea (NO. 18S-0709).

possible to achieve a maximum PCE of 11.4% because of the improvements to V_{oc} and J_{sc}. All the photovoltaic parameters are dramatically better in the P(Cl):ITIC-Th device because of the Cl substitution. Based on the properties of the polymers,

the higher V_{oc} of the P(Cl):ITIC-Th device can be attributed to the dramatically lower HOMO of P(Cl) with respect to that of P(Th).[5] For the other two photovoltaic parameters (J_{sc} and FF), the improvements may be due to well-matched energy level

Table 3. Photovoltaic performance of the optimized polymer blends for inverted PSCs.

Active layer[a]	V_{oc} [V]	J_{sc} [mA cm^{-2}]	FF [%]	PCE$_{max}$/PCE$_{ave}$[b] [%]
P(Th):ITIC-Th = 1:1.25 (1.2 wt%)	0.779	8.8	37.3	2.6/2.0 ± 0.60
P(Cl):ITIC-Th = 1:1.25 (1.2 wt%)	0.859	18.2	68.9	10.8/10.7 ± 0.11
P(Cl):ITIC-Th = 1:1.25 (1.2 wt%)[c]	0.899	18.6	68.1	11.4/11.2 ± 0.21
P(Cl):ITIC-Th = 1:1.25 (1.2 wt%)[d]	0.905	20.63	65.0	12.14

[a]Processed in CB/DIO (95:0.5, v/v) and coated at a 120 nm thickness and then annealed at 110 °C for 10 min; [b]Average PCE values are calculated from ten independent cells; [c]Measured with encapsulation in an air atmosphere after aging for 246 h; [d]Certification result from the NCPAC, Republic of Korea (No. 18S-0709).

alignment (offsets of HOMO and LUMO energy levels) and phase separation in their morphology, among other reasons.[5,6,21,36]

The EQE curves of the optimized devices (Figure 3b) are very similar in shape, but the P(Cl):ITIC-Th device shows superior efficiency in the entire response region. The P(Th):ITIC-Th device had a low EQE response of less than 50% in all regions in the range of 300–800 nm, but the P(Cl):ITIC-Th device had a high EQE response with a maximum value of more than 78%. Thus, the high J_{sc} of P(Cl) led to large efficiency improvements. The EQE response of the P(Cl):ITIC-Th device in the 300–500 nm region was slightly reduced after encapsulation and aging for 246 h. However, the maximum EQE response of 80% occurred in the low-energy region (550–800 nm) only after encapsulation and aging, because of the improved J_{sc} value. The current–density values integrated from the EQE spectra under the AM 1.5G spectrum are 9.0 mA cm^{-2} for the P(Th):ITIC-Th device, 16.98 mA cm^{-2} for the P(Cl):ITIC-Th pristine device, and 17.84 mA cm^{-2} for the P(Cl):ITIC-Th device that had undergone encapsulation after aging for 246 h. These are fairly consistent with the J_{sc} values obtained from the J–V curves (within 4%–7% mismatch), indicating the reliability of the measured J_{sc} data. To check the reliability of the best device for P(Cl):ITIC-Th with encapsulation after aging for 246 h, we requested measurements from the Nano Convergence Practical Application Center (NCPAC), Republic of Korea (NO. 18S-0709) for certification. As shown in Figure 3d, a maximum certified PCE of 12.14% was recorded (Figure S19, Supporting Information). To the best of our knowledge, this is the highest certified result for a single-junction PSC with mild temperature annealing below 110 °C. In fact, the majority of all fabricated devices require a drying process with mild-temperature annealing to remove the solvents and form a steady film of the active layer in a continuous roll-to-roll process for PSC module fabrication.[3,37–39] Thus, our results represent an opportunity for a significant contribution to the industrial production of PSCs in the near future.

We next investigated the stability of P(Cl):ITIC-Th both without and with encapsulation (Figure 3c). The encapsulation used was merely an epoxy adhesive (XNR5570) to protect from oxygen and moisture, and it performed more precisely comparison for their stability. The stability was studied by storing the devices in

an air-conditioned environment at room temperature and AM 1.5G under ambient conditions for over 2000 h, and subsequently, the international summit on organic photovoltaics stability in dark testing-1 (ISOS-D-1) shelf protocol was implemented.[13,40,41] As a gauge of device stability, the J–V characteristics of P(Cl):ITIC-Th without and with encapsulation were evaluated as a function of storage time in terms of the corresponding photovoltaic parameters (Figure S20, Supporting Information). The effect of aging on the photovoltaic parameters of the PSCs during long-term storage, without and with encapsulation, is clearly demonstrated. The performances of the devices gradually increased for up to 167 and 246 h, respectively, at which point the maximum PCEs were observed (without encapsulation: PCE = 11.3%, V_{oc} = 0.899 V, J_{sc} = 18.5 mA cm^{-2}, and FF = 67.6%; with encapsulation: PCE = 11.4%, V_{oc} = 0.899 V, J_{sc} = 18.6 mA cm^{-2}, and FF = 68.1%). We believe that the cause of this increase is the relaxation of the tilting generated by the presence of large Cl atoms in the polymer backbone; both devices have closer inter-/intramolecular packing order than their initial states.[33,42] Moreover, surprisingly, the PCEs of the cells without and with encapsulation retain 91% and 101% of their initial values for up to 2002 and 2858 h, respectively. The stability of the device without encapsulation is lower than that with encapsulation, but, this is considered to be caused by external factors such as moisture and oxygen during long-term storage under ambient conditions.[43] Also, we investigated the photostability of both devices under AM 1.5G continuous white light-emitting diode (LED) illumination. We adopted the LED as the light source instead of the xenon lamp used in the solar simulator due to light stability issues with reliability. The main emission spectrum of the LED lamp is restricted to 400–700 nm of the visible region and controlled to be 100 mW cm^{-2}. Initial performances of devices were tested from the xenon lamp and then compared with that of the LED lamp. The performance of devices between the xenon and LED lamps showed a difference of ≥1% PCEs due to the inherent light properties such emission spectrum in each different region. During the photostability measurements, both devices were operated continuously under the maximum output states and were naturally heated by the incident light to be ≈50 °C. The PCEs of both cells slightly decreased below 10%–12% compared with each initial PCE for 40 h, which means that the P(Cl):ITIC-Th-based devices have a high photostability regardless of the encapsulation. The results of the measurements are shown and summarized in Figure S21, Supporting Information. Nevertheless, these results for the P(Cl):ITIC-Th devices show that, with or without encapsulation, they have better atmospheric stability and photostability than the previously reported donor polymers.[13,33,40,41]

2.4. Microstructure Ordering and Morphological Characterization

As shown in **Figure 4**, 2D grazing-incidence wide-angle X-ray scattering (2D GIWAXS) is an efficient approach to investigate the crystallinity and molecular orientation of the pristine and blended polymer films. The 2D GIWAXS patterns (Figure 4a–d) and the corresponding out-of-plane (OOP; along q_{xy}) and in-plane (IP; along q_z) profiles (Figure 4e,f) of the four films, P(Th),
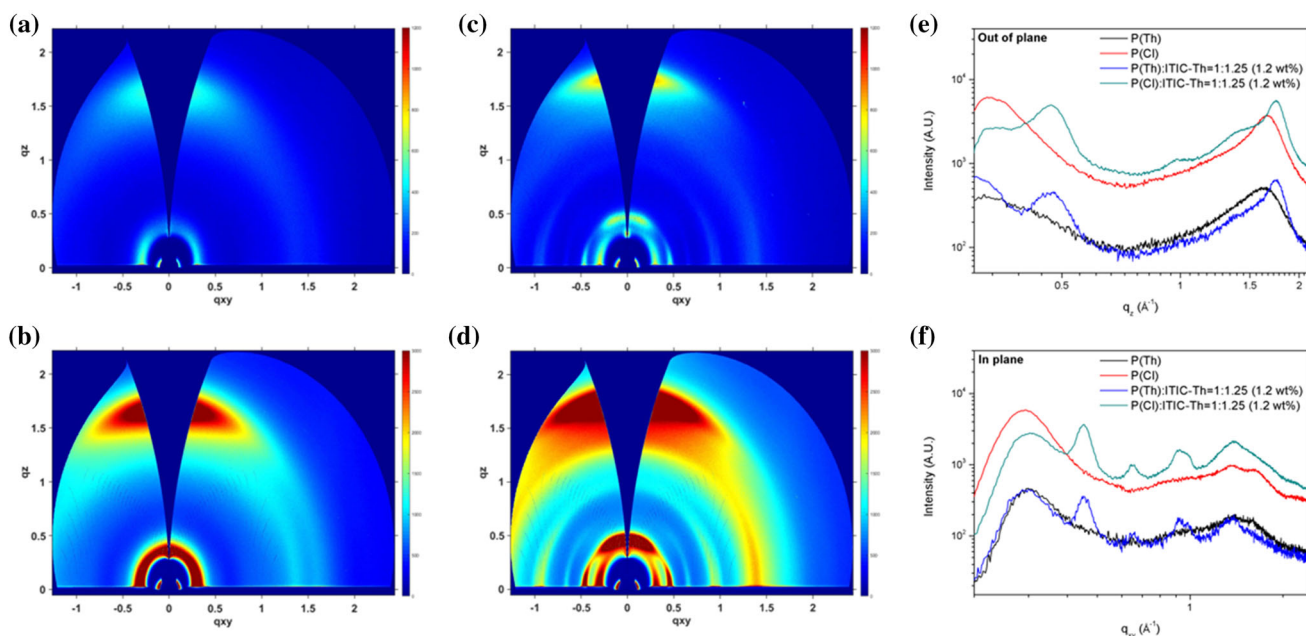
Figure 4. 2D-GIWAXS data for the pristine and blended polymers in the optimized conditions. The 2D-GIWAXS patterns for a) P(Th), b) P(Cl), c) P(Th):ITIC-Th, and d) P(Cl):ITIC-Th. e) OOP and f) IP GIWAXS profiles.

P(Th):ITIC-Th, P(Cl), and P(Cl):ITIC-Th, were obtained. Both pristine polymers show similar orientations on the ZnO substrate; face-on structures are manifested by the clear (010) peaks at 1.5–2.0 Å^{-1} in the OOP direction (Figure 4a,b). However, edge-on structures with intense (100) peaks at 0.2–0.5 Å^{-1} in the OOP direction occurred because of an increase in the crystallinity of the molecular structure caused by the introduction of Cl in the P(Cl) polymer backbone.[16–18] In addition, the introduction of chlorothiophene (which has an asymmetric structure) increases the number of regiorandom segments in the polymer backbone, compared with thiophene, which has a symmetric structure. Thus, the polymer with chlorothiophene has an amorphous nature, with peaks at 1.25–1.5 Å^{-1} in the OOP and IP directions.[15,22,24,26] As shown in Figure 4c,d, the trends are similar for the corresponding polymer blends. Both blends have enhanced π—π stacking properties compared with the pristine films by introducing ITIC-Th. Not only does the P(Th):ITIC-Th blend film maintains its π—π stacking, but the lack of lamellar packing in the OOP and IP directions is also retained. P(Cl):ITIC-Th showed higher crystallinity and π—π stacking than the pristine P(Cl) film in the OOP and IP profiles.

Detailed parameters from the profiles of the films are presented in **Table 4**. To better understand these trends, the pristine ITIC-Th film was subjected to GIWAXS, and the resulting data, plotted as OOP and IP profiles, are presented in the Supporting Information (Figure S22, Supporting Information). Furthermore, the OOP data for the pristine and blended polymers from GIWAXS results are summarized in Table 4. As shown in Figure 4e,f, in the films of the pristine polymers, the (100) and (010) distances for P(Cl) became closer to 1.0 and 0.07 Å, respectively, closer than the equivalent values for P(Th). Considering the films of the polymer blended with ITIC-Th, P(Cl):ITIC-Th also retained a high degree of lamellar packing and π—π stacking to a greater extent than P(Th):ITIC-Th, and the (100) and (010) distances in the former film were closer at 2.23 and 0.01 Å, respectively.[15,42] Considering the (100) and (200) peaks, which demonstrated the crystallinity of ITIC-Th, we can conclude that P(Cl):ITIC-Th has a longer-range packing order than P(Th):ITIC-Th; the (100) distance becomes as small as 0.05 Å, and the (200) peak is seen only for P(Cl):ITIC-Th, taking a distance of 6.37 Å.[44–46] These results agree well with previously analyzed trends.

Table 4. GIWAXS results for pristine and blended polymers in the OOP direction.

Conditions	d[100] [Å] at (100) [Å^{-1}]	d[100]$_{ITIC-Th}$ [Å] at ITIC-Th (100) [Å^{-1}]	d[200]$_{ITIC-Th}$ [Å] at ITIC-Th (200) [Å^{-1}]	d[010]$^{a)}$[Å] at (010) [Å^{-1}]
P(Th)	19.74 at 0.318	—	—	3.85 at 1.632
P(Cl)	18.74 at 0.335	—	—	3.78 at 1.663
P(Th):ITIC-Th	20.74 at 0.303	13.37 at 0.470	—	3.60 at 1.744
P(Cl):ITIC-Th	18.51 at 0.339	13.32 at 0.472	6.37 at 0.986	3.59 at 1.750

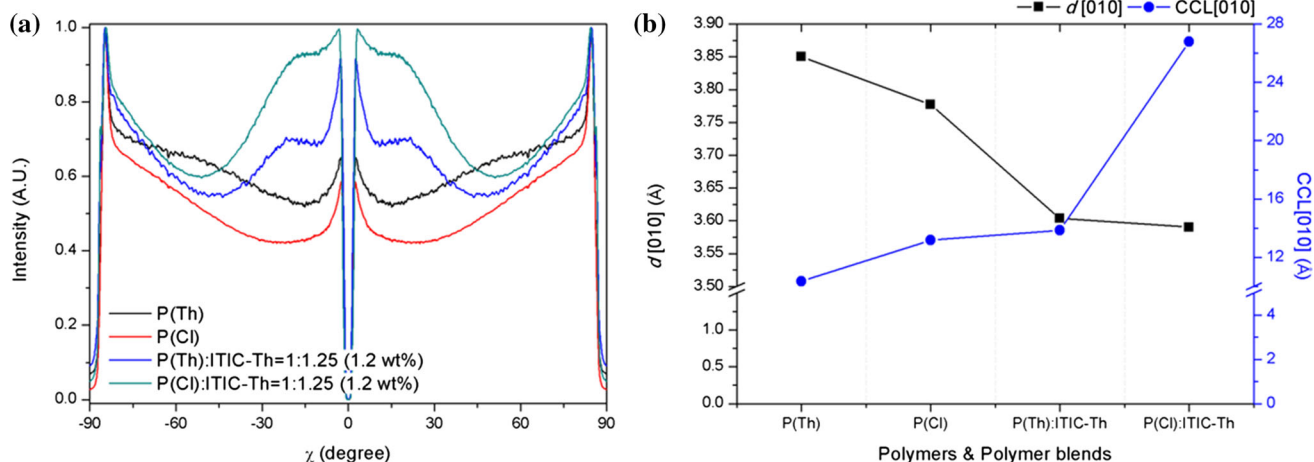$^{a)}q_{xy}$ (or q_z) = $2\pi/d$[010] (or d[h00]).

Figure 5. a) Integrated pole figure plots for the (100) lamellar diffraction and b) π—π stacking distance (d[010]) and coherence lengths (CCL[010]) estimated from the (010) π—π stacking diffraction in the OOP direction, respectively, for the pristine and blended polymers.

In addition, we constructed intensity-integrated azimuthal pole figure plots for the (100) scattering peaks of the pristine and blended polymer films (**Figure 5**a). The integrated areas within the azimuthal angle (χ) in the ranges of 0–45° (A_z) and 45–90° (A_{xy}) are defined as the corresponding fractions of face-on and edge-on structures, respectively, and the ratio A_{xy}/A_z was calculated as a metric for the face-on-to-edge-on ratio. P(Cl) has a higher A_{xy}/A_z value (1.29) than P(Th) (1.17), suggesting the existence of a larger population of face-on structures;[47,48] it should be noted, however, that the values of A_{xy}/A_z for the blended P(Th) and P(Cl) films are reduced (0.98 and 0.82, respectively) compared with those of the respective pristine films. These A_{xy}/A_z results mean that P(Cl):ITIC-Th has higher crystallinity than P(Th):ITIC-Th, which probably boosts its charge carrier mobility.[47–49] Next, we determined the π—π stacking distance (d[010]) and the coherence lengths (CCL[010]) using the OOP (010) peaks (Figure 5b); linear trends, both for the pristine and blend films, are observed. P(Cl) has a larger CCL, with a smaller π—π stacking distance, compared with P(Th). This difference was clearer in the blended-polymer films, establishing that P(Cl):ITIC-Th has a higher crystallinity with tighter π—π stacking than P(Th):ITIC-Th.[50,51] These results are beneficial for charge-carrier transport in the vertical channels across the electrodes;[47–51] the parameters are summarized in the Supporting Information (Table S8, Supporting Information).

The surface and micro/nanoscale morphologies of both polymer-blend films were measured using atomic force microscopy (AFM) and transmission electron microscopy (TEM). The polymer-blend films were prepared under the same conditions as for device fabrication. As shown in **Figure 6**a–d, P(Th):ITIC-Th exhibits a distinctly aggregated surface and very large islands with large microscale separated domains (root-mean-square [RMS], $R_q = 2.00$ nm, and the maximized roughness in the z-axis direction, $R_z^{max} = 33.94$ nm).[19] In contrast, the P(Cl):ITIC-Th shows smooth and uniform features, with a smaller surface roughness ($R_q = 1.26$ nm and $R_z^{max} = 10.06$ nm). Fine-dispersed surfaces with nanoscale structures are known to result in more charge separation and transport.[10,16,17,36] Moreover, relatively reduced surface roughness can enable a defect-free contact with the MoO_3 layer, resulting in increased FF and J_{sc} values.[5,10,36]

TEM images of both the polymer-blend films exhibit truly continuous nanosized domain structures (**Figure 7**a,c; Figure S23, Supporting Information). In general, nanophase separation morphologies of polymer blend films are determined by aggregation effects of the polymers.[36] Here, no large aggregates for P(Cl):ITIC-Th can be observed, even by comparison of the expanded TEM images shown in Figure 7b,d. This means that the P(Cl):ITIC-Th film is much more homogeneous than the P(Th):ITIC-Th film at the nanoscaled networks.[10,13–15] Such homogeneity is known to be favorable for effective exciton diffusion, charge separation, and charge transport because it allows the formation of continuous charge-transport channels,[10,14,36] and hence, this result indicates a higher FF and J_{sc} for P(Cl)-based PSCs.

To examine the combined donor–acceptor states, we also measured the energy-dispersive X-ray (EDX) elemental mapping for both the polymer-blend films. In **Figure 8**a,b, the green, white, yellow, and red dots indicate sulfur, oxygen, nitrogen, and chlorine, respectively, in the EDX maps of the polymers blended with ITIC-Th (Scheme S2 and Figure S24, Supporting Information). The S map clearly reveals the interconnecting network between the polymers and ITIC-Th, whereas the O and N maps indicate the ITIC-Th distribution in both films.[24,47] These map results demonstrate the internal uniformity of the dispersion of two components in both films.[14] Interestingly, the Cl signals only appear in P(Cl), proving that their polymer backbone still contains chlorine atoms after the Stille C–C coupling polymerization, which occurs without competition between Cl and Br ligands. The EDX Cl mapping results visually prove that the enhanced performance is caused by the effect of chlorine in the P(Cl) backbone.

2.5. Charge-Transport Properties

Charge transfer between the donors and the acceptors, in both polymer-blend films, needs to be further investigated to clarify its contribution to the device performance. Photoluminescence (PL) measurement is a convenient tool for probing charge transfer or
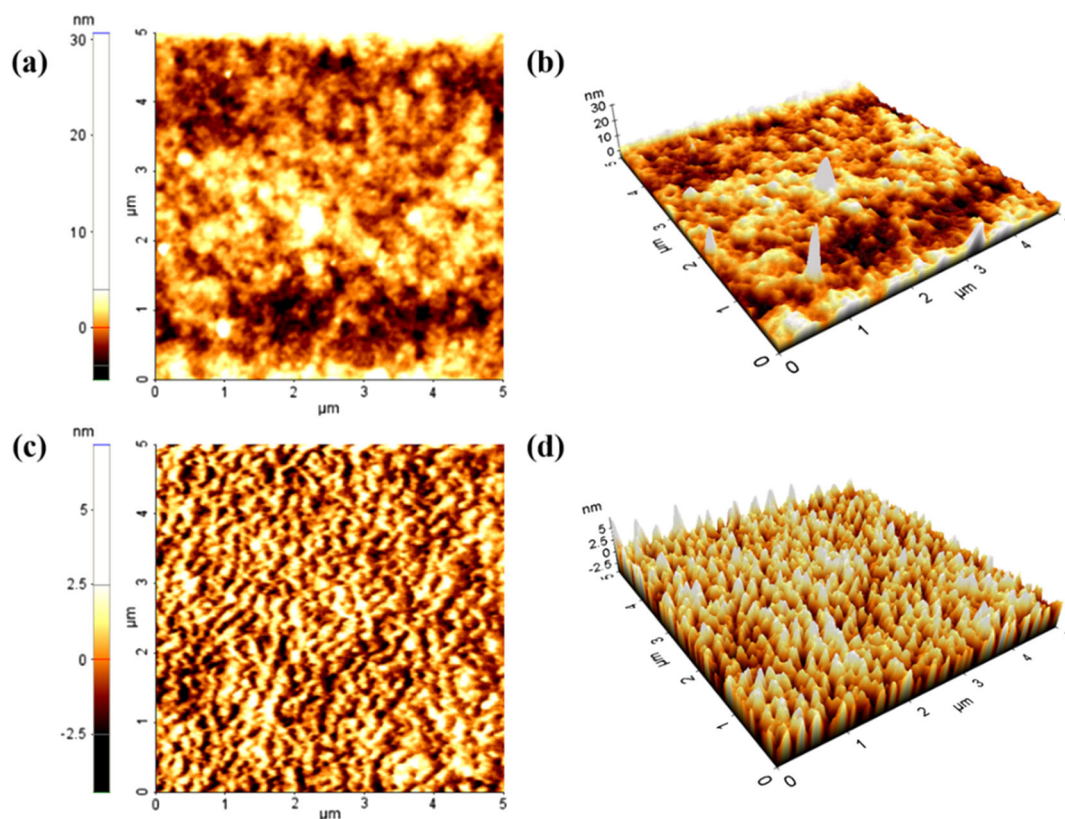
Figure 6. AFM images of the optimized polymer blends: a,c) 2D and b,d) 3D topography for a,b) P(Th):ITIC-Th and c,d) P(Cl):ITIC-Th.
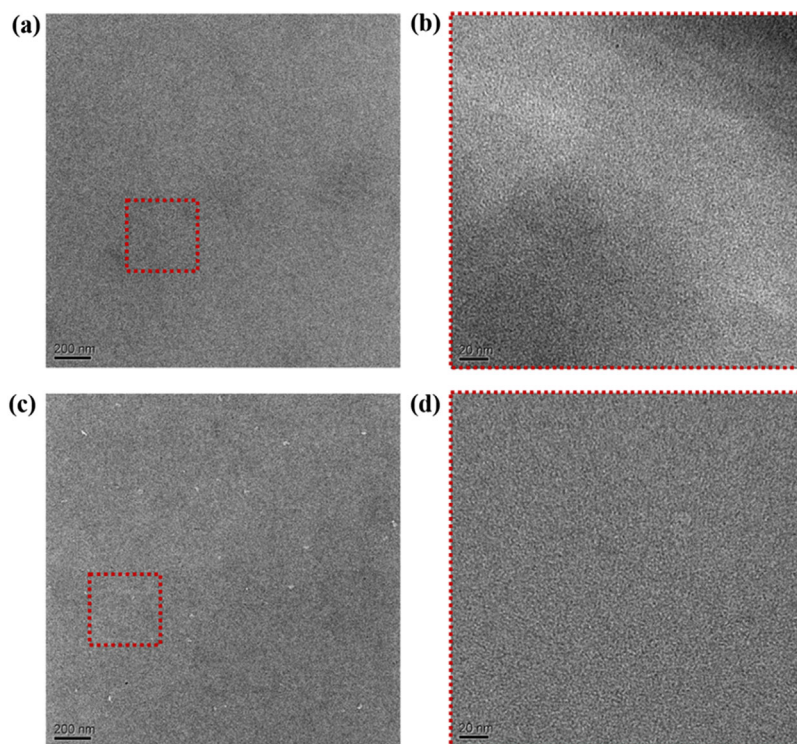

Figure 7. TEM images of the optimized polymer blends: a,b) P(Th):ITIC-Th and c,d) P(Cl):ITIC-Th; (b) and (d) are expanded views of the areas marked by red dashed outline overlays in (a) and (c), respectively.
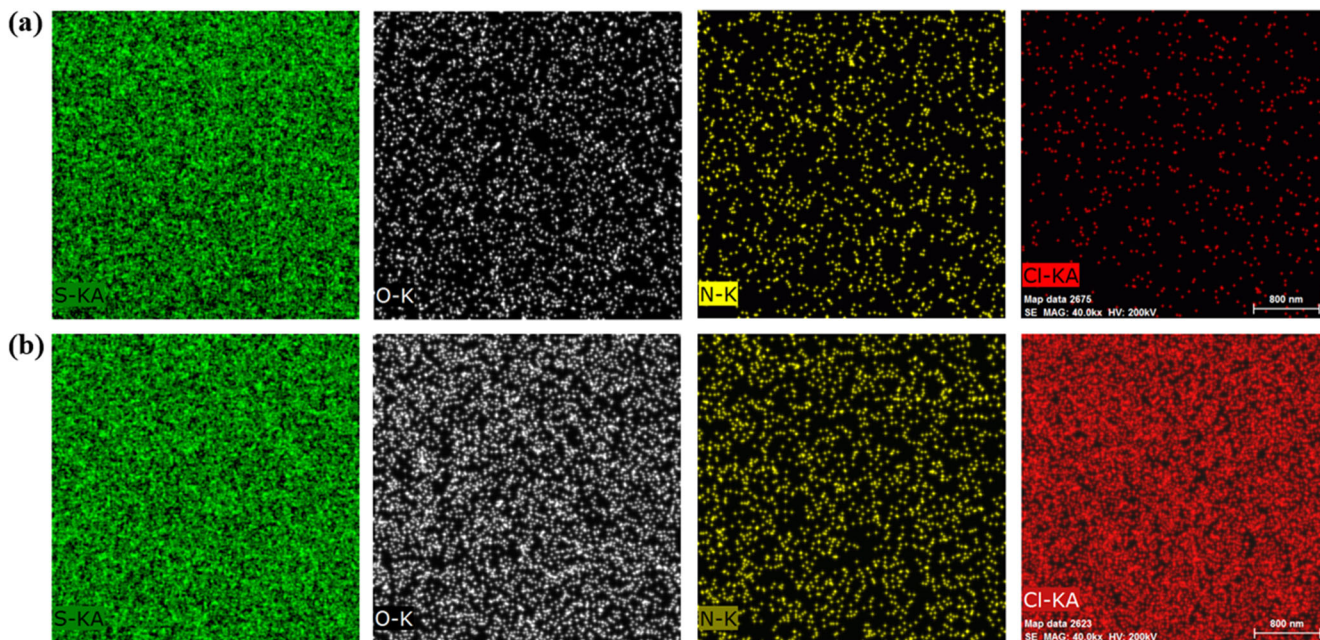
Figure 8. EDX images of the optimized polymer blends: a) P(Th):ITIC-Th and b) P(Cl):ITIC-Th.

energy transfer between each materials; thus, it was performed for the materials in this study[13,40] (Figure S25, Supporting Information). The polymers and ITIC-Th have PL emission in the regions of 600–800 nm and 650–850 nm, respectively; in contrast, in the polymer blends, an effective PL quenching behavior is clearly observed at 650–850 nm. P(Th):ITIC-Th showed insufficient quenching rates, 80% and 34% upon excitation at 500 nm (polymer) and 630 nm (ITIC-Th), respectively. In contrast, the PL spectra of P(Cl):ITIC-Th showed that a highly efficient photoinduced charge transfer occurs, with relatively high quenching rates of 97% and 95%, with excitation at 500 and 630 nm, respectively.[13,14,33,47] These results are consistent with the trend of EQE values for both the PSC polymer blends.

Furthermore, we measured the space-charge-limited current (SCLC) of hole-only and electron-only devices to verify the charge-carrier mobilities in both polymer blends (Figure S26 and Table S9, Supporting Information). The resulting electron and hole mobilities (μ_e and μ_h) were calculated as 2.11×10^{-6} and 6.63×10^{-5} cm^2 V^{-1} s^{-1} for P(Th):ITIC-Th and as 5.12×10^{-4} and 3.41×10^{-4} cm^2 V^{-1} s^{-1} for P(Cl):ITIC-Th, using the modified Mott–Gurney equation (see the Supporting Information for more details). The calculation results showed that P(Cl):ITIC-Th has higher electron and hole mobilities than P(Th):ITIC-Th by two and one orders of magnitude, respectively, and their electron/hole mobilities (μ_e/μ_h) are approximately 21.7 times more balanced than those of P(Th):ITIC-Th. This result has beneficial implications for the suppression of space-charge accumulation and thus for the promotion of charge extraction, contributing to the enhanced performance of P(Cl):ITIC-Th.[13–17,21,26,33]

2.6. Cost Effectiveness of P(Cl)

In 2015, Po et al. systematically overviewed various classes of donor polymers to define the SC, which can be used for

designing simple and high-performance PSC materials in terms of the number for synthetic steps, overall yields, operations, and purifications, as well as to avoid the use of hazardous chemicals in their preparation[11,12] (see Supporting Information for details). Despite much success in some aspects of their performance, in general, the SC of the donor polymers required to produce such device performance render them incompatible with the industrialization of PSCs. It has been stated that the final commercialized donor materials should have an acceptable trade-off between PCE and SC.[11,12]

Therefore, we also investigated and analyzed the SC for P(Cl) to insert our data into the Po group's study, as shown in **Figure 9**a (Scheme S1 and Table S10, Supporting Information). Figure 9a shows the data on an adjusted y-axis scale to definitely see the 105 types of donor polymers with PCEs of >4.9%, based on fullerene acceptors. As the plot changes from green to red, the donor polymers become less cost effective. Although P(Th) has a low SC (31.3%), it cannot be ranked in Figure 9a because of its low PCE (2.6%). SC values of the commercialized donor polymers P3HT, PTB7, PTB7-Th, and PBDB-T are 7.7%, 58.8%, 64.3%, and 47.9%, respectively, whereas P(Cl) has an SC of 36.7%. In particular, the polymers occupying the green region of the plot in Figure 9a, such as P3HT and P(Cl), are those for which the relationship between PCE and cost is reasonable.[11,12]

As shown in Figure 9b, we surveyed and calculated a figure of merit (FOM-n = SC/PCE$_{nonfullerene}$) and a PCE based on NFAs (PCE$_{nonfullerene}$) for the commercial polymers and P(Cl). We obtained PCE$_{nonfullerene}$ values for P3HT, PTB7-Th, and PBDB-T, in each case, as the highest recorded performance based on an NFA in a binary-component single cell, as found in the most recently published literature[40,41,52,53] (Table S10, Supporting Information). Each polymer is ranked according to its FOM-n based on its SC and PCE, and some issues relating to the design of the materials, along with some insights about the syntheses,
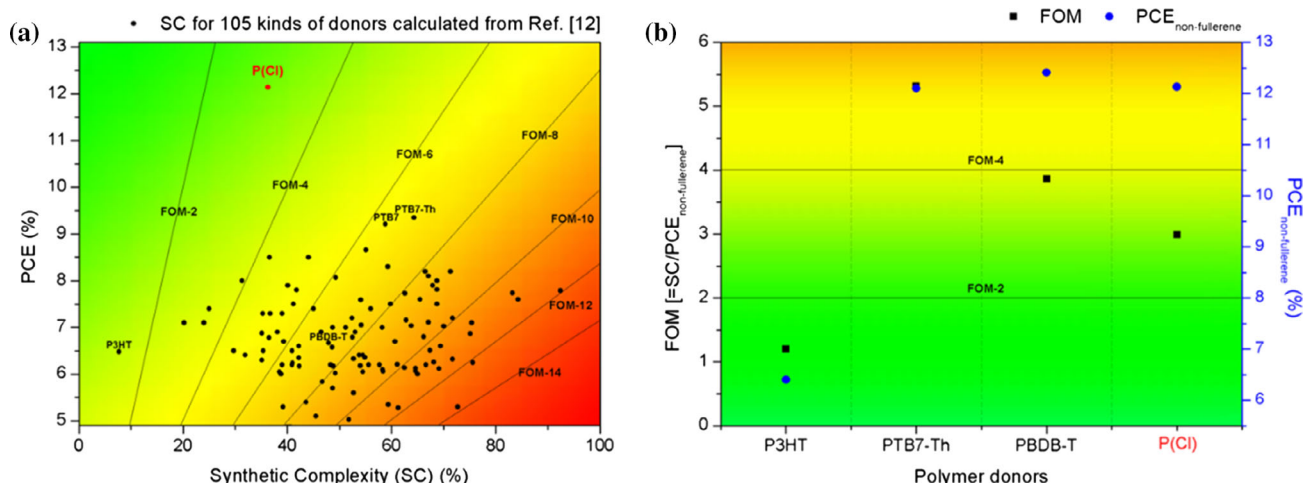
Figure 9. a) PCE and synthetic complexities of P(Cl) and 105 reported donors with PCEs > 4.9%, based on fullerene-acceptor polymers and b) FOM-n and PCE values with NFAs for commercial donor polymers and P(Cl):ITIC-Th. Adapted with permission.[12] Copyright 2017, Wiley.

are now discussed. The FOM-n (black squares) with $PCE_{nonfullerene}$ (blue circles) values for P3HT, PTB7-Th, PBDB-T, and P(Cl) are FOM-1 with 6.4%, FOM-5 with 12.1%, FOM-4 with 12.41%, and FOM-3 with 12.14%, respectively. The larger interval between the FOM and the $PCE_{nonfullerene}$ of P(Cl) indicates that it represents the best cost-efficiency balance among all the commercial donor polymers, with the exception of P3HT, which sits in the green region of the plots in Figure 9.[11,12] Thus, we believe that P(Cl) will be a promising donor polymer for the commercial application of PSCs.

3. Conclusions

In conclusion, two heterocyclic ring-based donor polymers, P(Th) and P(Cl), were designed and synthesized via approaches with low synthetic complexities. Various advantages of these syntheses include high overall yields, low number of synthetic steps, and use of inexpensive raw materials. Compared with P(Th), in which there is no Cl substitution, P(Cl) showed enhanced physical, optical, and electrochemical properties, such as molecular weight, dipole moment, and absorption coefficient. In particular, P(Cl) has a wide bandgap of 1.97 eV and a low-lying HOMO energy level at −5.47 eV. Thus, P(Cl) has well-matched energy-level alignment and complementary optical absorption with non-fullerene narrow-bandgap acceptors, specifically, with ITIC-Th. Inverted-structure PSCs based on P(Cl):ITIC-Th were shown to have PCE values of up to 12.14%. Moreover, P(Cl):ITIC-Th devices fabricated without and with encapsulation exhibited superior long-term stability: the PCE value was maintained at 91% and 100% of its initial value, for up to 2002 and 2858 h, respectively, under ambient conditions. We believe that P(Cl) will be a promising donor polymer for the commercial application of PSCs. To the best of our knowledge, this study is the first successful attempt of synthesizing D–A conjugated polymers containing Cl, even if Cl and Br with competitive reactivity are simultaneously introduced during polymerization. Furthermore, as a tool for a polymer structure design, the results of this study

will shed new light on the chemistry of heterocyclic rings with various substituted electron-withdrawing groups that have thus far been ignored because of preconceptions regarding chemical reactivity.

4. Experimental Section

Polymerization: Scheme 1 outlines the synthetic routes for the polymers. The detailed synthetic procedures with characterization results for the monomers, M1, M2, and dibromo Th–Cl, and polymers, P(Th) and P(Cl), are shown in the Supporting Information (Figure S1–S5, Supporting Information).

Poly[(2,6-(4,8-bis(5-(2-ethylhexyl)thiophen-2-yl)-benzo[1,2-b:4,5-b']dithiophene))-alt-(2,5-(3-chlorothiophene))] (P(Cl)) and P(Th): To a mixture of monomer dibromo Th–Cl or M2 (0.2 mmol), M1 (180.0 mg, 0.199 mmol) and Pd(pph$_3$)$_4$ (8.0 mg) were added in a 10–20 mL vial in air. The vial was capped and vacuumed for 20 min before it was refilled with nitrogen gas, and then, anhydrous toluene (6.0 mL) was added to the mixture. The reactor was degassed and refilled with nitrogen twice. The polymerization mixture was stirred at 100 °C for 3 h. The polymer was end-capped by the addition of 2-bromothiophenes (56.0 mg, 0.33 mmol), and the mixture was further heated at 140 °C for 1 h. After heating, 2-tributylstannyl thiophene (31.3 mg, 0.0875 mmol) was added, and the mixture was heated once more at 140 °C for 1 h. The reaction mixture was cooled to room temperature and poured into methanol (300 mL) and 37% HCl (10 mL), stirred for 1 h, and then further purified using a Soxhlet extractor with methanol, acetone, hexane, methylene chloride, ethyl acetate, and CF, sequentially. The CF fraction of P(Cl) was reprecipitated in methanol, filtered, and then dried under vacuum.

P(Cl): (dark red solid, yield: 90%) ^{1}H NMR (400 MHz, CDCl$_3$, δ): 7.52–6.88 (br, 7H), 2.96–2.94 (br, 4H), 1.88–0.71 (br, 30H). Anal. calc. found for $C_{38}H_{43}ClS_5$: C 65.62, H 6.23, Cl 5.10, S 23.05; Elemental analysis (EA) found, C 68.75, H 8.77, S 21.25.

P(Th): (bright red solid, yield: 67%) ^{1}H NMR (400 MHz, CDCl$_3$, δ): 7.00–6.94 (br, 8H), 2.97–2.94 (br, 4H), 1.80–0.84 (br, 30H). Anal. calc. found for $C_{38}H_{44}S_5$: C 69.04, H 6.71, S 24.25; Elemental analysis (EA) found, C 70.20, H 7.55, S 22.11.

Supporting Information

Supporting Information is available from the Wiley Online Library or from the author.

[1] V. Shrotriya, *Nat. Photon.* **2009**, *3*, 447.

[2] S. R. Forrest, *Nature* **2004**, *428*, 911.

[3] R. Søndergaard, M. Hösel, D. Angmo, T. T. Larsen-Olsen, F. C. Krebs, *Mater. Today* **2012**, *15*, 36.

[4] G. Zhang, J. Zhao, P. C. Y. Chow, K. Jiang, J. Zhang, Z. Zhu, J. Zhang, F. Huang, H. Yan, *Chem. Rev.* **2018**, *118*, 3447.

[5] S. Zhang, Y. Qin, J. Zhu, J. Hou, *Adv. Mater.* **2018**, *30*, 1800868.

[6] H. Zhang, H. Yao, J. Hou, J. Zhu, J. Zhang, W. Li, R. Yu, B. Gao, S. Zhang, J. Hou, *Adv. Mater.* **2018**, *30*, 1800613.

[7] L. Meng, Y. Wang, X. Wan, C. Li, X. Zhang, Y. Wang, X. Ke, Z. Xiao, L. Ding, R. Xia, H.-L. Yip, Y. Chen, *Science* **2018**, *361*, 1094.

[8] J. Yuan, Y. Zhang, L. Zhou, G. Zhang, H.-L. Yip, T.-K. Lau, X. Lu, C. Zhu, H. Peng, P. A. Johnson, M. Leclerc, Y. Cao, J. Ulanski, Y. Li, Y. Zou, *Joule* **2019**, *3*, 1.

[9] J. Yuan, T. Huang, P. Cheng, Y. Zou, H. Zhang, J. L. Yang, S.-Y. Chang, Z. Zhang, W. Huang, R. Wang, D. Meng, F. Gao, Y. Yang, *Nat. Commun.* **2019**, *10*, 570.

[10] J.-Y. Kim, S. Park, S. Lee, H. Ahn, S.-Y. Joe, B. J. Kim, H. J. Son, *Adv. Energy Mater.* **2018**, *8*, 1801601.

[11] R. Po, J. Roncali, *J. Mater. Chem. C* **2016**, *4*, 3677.

[12] R. Po, G. Bianchi, C. Carbonera, A. Pellegrino, *Macromolecules* **2015**, *48*, 453.

[13] G. E. Park, S. Choi, S. Y. Park, D. H. Lee, M. J. Cho, D. H. Choi, *Adv. Energy Mater.* **2017**, *7*, 1700566.

[14] Y. Firdaus, L. Pratali Maffei, F. Cruciani, M. A. Müller, S. Liu, S. Lopatin, N. Wehbe, G. O. N. Ndjawa, A. Amassian, F. Laquai, P. M. Beaujuge, *Adv. Energy Mater.* **2017**, *7*, 1700834.

[15] D. Xia, Y. Wu, Q. Wang, A. Zhang, C. Li, Y. Lin, F. J. M. Colberts, J. J. Van Franeker, R. A. J. Janssen, X. Zhan, W. Hu, Z. Tang, W. Ma, W. Li, *Macromolecules* **2016**, *49*, 6445.

[16] Z. Ji, X. Xu, G. Zhang, Y. Li, Q. Peng, *Nano Energy* **2017**, *40*, 214.

[17] D. Mo, H. Wang, H. Chen, S. Qu, P. Chao, Z. Yang, L. Tian, Y.-A. Su, Y. Gao, B. Yang, W. Chen, F. He, *Chem. Mater.* **2017**, *29*, 2819.

[18] Y. Wang, Y. Zhang, N. Qiu, H. Feng, H. Gao, B. Kan, Y. Ma, C. Li, X. Wan, Y. Chen, *Adv. Energy Mater.* **2018**, *8*, 1702870.

[19] T. L. Nguyen, H. Choi, S.-J. Ko, M. A. Uddin, B. Walker, S. Yum, J.-E. Jeong, M. H. Yun, T. J. Shin, S. Hwang, J. Y. Kim, H. Y. Woo, *Energy Environ. Sci.* **2014**, *7*, 3040.

[20] S. J. Jeon, S. J. Nam, Y. W. Han, T. H. Lee, D. K. Moon, *Polym. Chem.* **2017**, *8*, 2979.

[21] W. Zhao, S. Li, H. Yao, S. Zhang, Y. Zhang, B. Yang, J. Hou, *J. Am. Chem. Soc.* **2017**, *139*, 7148.

[22] L. Ying, F. Huang, G. C. Bazan, *Nat. Commun.* **2017**, *8*, 14047.

[23] J. E. Coughlin, A. Zhugayevych, M. Wang, G. C. Bazan, S. Tretiak, *Chem. Sci.* **2017**, *8*, 1146.

[24] Y. Jin, Z. Chen, S. Dong, N. Zheng, L. Ying, X. F. Jiang, F. Liu, F. Huang, Y. Cao, *Adv. Mater.* **2016**, *28*, 9811.

[25] E. Collado-Fregoso, P. Boufflet, Z. Fei, E. Gann, S. Ashraf, Z. Li, C. R. McNeill, J. R. Durrant, M. Heeney, *Chem. Mater.* **2015**, *27*, 7934.

[26] H. Zhong, C. Z. Li, J. Carpenter, H. Ade, A. K. Y. Jen, *J. Am. Chem. Soc.* **2015**, *137*, 7616.

[27] H. Luo, C. Yu, Z. Liu, G. Zhang, H. Geng, Y. Yi, K. Broch, Y. Hu, A. Sadhanala, L. Jiang, P. Qi, Z. Cai, H. Sirringhaus, D. Zhang, *Sci. Adv.* **2016**, *2*, e1600076.

[28] H. Yao, D. Qian, H. Zhang, Y. Qin, B. Xu, Y. Cui, R. Yu, F. Gao, J. Hou, *Chin. J. Chem.* **2018**, *36*, 491.

[29] H. I. Kim, M. Kim, C. W. Park, H. U. Kim, H. K. Lee, T. Park, *Chem. Mater.* **2017**, *29*, 6793.

[30] T. Vangerven, P. Verstappen, J. Drijkoningen, W. Dierckx, S. Himmelberger, A. Salleo, D. Vanderzande, W. Maes, J. V. Manca, *Chem. Mater.* **2015**, *27*, 3726.

[31] J. Lee, M. Malekshahi Byranvand, G. Kang, S. Y. Son, S. Song, G. W. Kim, T. Park, *J. Am. Chem. Soc.* **2017**, *139*, 12175.

[32] W. Lee, H. Cha, Y. J. Kim, J. E. Jeong, S. Hwang, C. E. Park, H. Y. Woo, *ACS Appl. Mater. Interfaces* **2014**, *6*, 20510.

[33] J. E. Yu, S. J. Jeon, J. Y. Choi, Y. W. Han, D. K. Moon, *Small*, **2019**, 1805321.

[34] M. H. Choi, K. W. Song, D. K. Moon, *Polym. Chem.* **2015**, *6*, 2636.

[35] Z. He, C. Zhong, S. Su, M. Xu, H. Wu, Y. Cao, *Nat. Photon.* **2012**, *6*, 593.

[36] Y. Huang, E. J. Kramer, A. J. Heeger, G. C. Bazan, *Chem. Rev.* **2014**, *114*, 7006.

[37] M. Helgesen, J. E. Carlé, G. A. Dos Reis Benatto, R. R. Søndergaard, M. Jørgensen, E. Bundgaard, F. C. Krebs, *Adv. Energy Mater.* **2015**, *5*, 1401996.

[38] J. E. Carlé, M. Helgesen, O. Hagemann, M. Hösel, I. M. Heckler, E. Bundgaard, S. A. Gevorgyan, R. R. Søndergaard, M. Jørgensen, R. García-Valverde, S. Chaouki-Almagro, J. A. Villarejo, F. C. Krebs, *Joule* **2017**, *1*, 274.

[39] S. Strohm, F. Machui, S. Langner, P. Kubis, N. Gasparini, M. Salvador, I. McCulloch, H. J. Egelhaaf, C. J. Brabec, *Energy Environ. Sci.* **2018**, *11*, 2225.

[40] S. Holliday, R. S. Ashraf, A. Wadsworth, D. Baran, S. A. Yousaf, C. B. Nielsen, C. H. Tan, S. D. Dimitrov, Z. Shang, N. Gasparini, M. Alamoudi, F. Laquai, C. J. Brabec, A. Salleo, J. R. Durrant, I. McCulloch, *Nat. Commun.* **2016**, *7*, 11585.

[41] D. Baran, R. S. Ashraf, D. A. Hanifi, M. Abdelsamie, N. Gasparini, J. A. Röhr, S. Holliday, A. Wadsworth, S. Lockett, M. Neophytou, C. J. M. Emmott, J. Nelson, C. J. Brabec, A. Amassian, A. Salleo, T. Kirchartz, J. R. Durrant, I. McCulloch, *Nat. Mater.* **2017**, *16*, 363.

[42] T. Zhang, G. Zeng, F. Ye, X. Zhao, X. Yang, *Adv. Energy Mater.* **2018**, *8*, 1801387.

[43] P. Cheng, X. Zhan, *Chem. Soc. Rev.* **2016**, *45*, 2544.

[44] Y. Lin, F. Zhao, Q. He, L. Huo, Y. Wu, T. C. Parker, W. Ma, Y. Sun, C. Wang, D. Zhu, A. J. Heeger, S. R. Marder, X. Zhan, *J. Am. Chem. Soc.* **2016**, *138*, 4955.

[45] J. Liu, L.-K. Ma, H. Lin, L. Zhang, Z. Li, W. K. Law, A. Shang, H. Hu, W. Ma, H. Yan, *Small Methods* **2018**, *2*, 1700415.

[46] H. Hu, K. Jiang, P. C. Y. Chow, L. Ye, G. Zhang, Z. Li, J. H. Carpenter, H. Ade, H. Yan, *Adv. Energy Mater.* **2018**, *8*, 1701674.

[47] J. Lee, D. H. Sin, B. Moon, J. Shin, H. G. Kim, M. Kim, K. Cho, *Energy Environ. Sci.* **2017**, *10*, 247.

[48] J. W. Jo, J. W. Jung, E. H. Jung, H. Ahn, T. J. Shin, W. H. Jo, *Energy Environ. Sci.* **2015**, *8*, 2427.

[49] L. Yang, S. Zhang, C. He, J. Zhang, Y. Yang, J. Zhu, Y. Cui, W. Zhao, H. Zhang, Y. Zhang, Z. Wei, J. Hou, *Chem. Mater.* **2018**, *30*, 2129.

[50] G. Zhang, X. Xu, Z. Bi, W. Ma, D. Tang, Y. Li, Q. Peng, *Adv. Funct. Mater.* **2018**, *28*, 1706404.

[51] Y. Lin, F. Zhao, Y. Wu, K. Chen, Y. Xia, G. Li, S. K. K. Prasad, J. Zhu, L. Huo, H. Bin, Z. G. Zhang, X. Guo, M. Zhang, Y. Sun, F. Gao, Z. Wei, W. Ma, C. Wang, J. Hodgkiss, Z. Bo, O. Inganäs, Y. Li, X. Zhan, *Adv. Mater.* **2017**, *29*, 1604155.

[52] J. Lee, S.-J. Ko, M. Seifrid, H. Lee, C. McDowell, B. R. Luginbuhl, A. Karki, K. Cho, T.-Q. Nguyen, G. C. Bazan, *Adv. Energy Mater.* **2018**, *8*, 1801209.

[53] Z. Fei, F. D. Eisner, X. Jiao, M. Azzouzi, J. A. Röhr, Y. Han, M. Shahid, A. S. R. Chesman, C. D. Easton, C. R. McNeill, T. D. Anthopoulos, J. Nelson, M. Heeney, *Adv. Mater.* **2018**, *30*, 1705209.

1900094 (14 of 14)